

# Detectability of a phantom-like braneworld model with the integrated Sachs-Wolfe effect

Tommaso Giannantonio <sup>\*</sup>, Yong-Seon Song <sup>†</sup> and Kazuya Koyama <sup>‡</sup>

*Institute of Cosmology & Gravitation, University of Portsmouth, Portsmouth, Hampshire, PO1 2EG, UK*

(Dated: November 11, 2018)

We study a braneworld model in which a phantom-like behaviour occurs with only cold dark matter and a cosmological constant, due to a large distance modification of gravity. With the addition of curvature, the geometrical tests are not strict enough to rule out models in which gravity is modified significantly on large scales. We show that this degeneracy in the parameter space is broken by the structure formation tests, such as the integrated Sachs-Wolfe effect, which can probe general relativity on large scales.

PACS numbers: 04.50.Kd, 95.36.+x, 98.80.Es

## I. INTRODUCTION

The late time acceleration of the Universe is one of the biggest problems in cosmology. In the framework of conventional general relativity, the expansion of the Universe at late times is dominated by a *dark energy* with negative pressure and equation of state  $w \equiv p/\rho < -1/3$ . Several current observations suggest  $w < -1$ , which is often called *phantom* dark energy, although the fiducial LCDM model with  $w = -1$  is still preferred if we combine all the data sets [1, 2]. From a theoretical point of view, it is extremely difficult to realise dark energy models with  $w < -1$ : the easiest way to obtain such a model is to consider a ghost scalar field with the wrong sign for the kinetic term, although this leads to the instability of the vacuum [3]. There are a few successful models that lead to  $w < -1$  without having theoretical pathologies [4, 5]; among them, we focus on a braneworld model proposed by Sahni and Shtanov [6] and further developed by Lue and Starkman [7].

This model is based on the Dvali–Gabadadze–Porrati (DGP) model of the 5D braneworld where we are supposed to live on a 4D brane in the 5D Minkowski spacetime [8]. The 4D gravity on the brane is recovered by the induced 4D Einstein–Hilbert action on the brane. In this model there are two branches of the solutions [9]: in the first branch, known as *self-accelerating*, the late time acceleration can be realised without introducing any dark energy, while in the other, known as the *normal* branch, a cosmological constant is needed to explain the late time accelerated expansion of the Universe; nevertheless, the extra-dimensional effects modify gravity on large scales and the model deviates from the standard LCDM. In particular, at the background level, the Universe behaves as if there were a phantom-like dark energy  $w < -1$ .

Besides the fact that this model mimics a phantom behaviour, it is known to be free of ghosts and thus rep-

resents a healthy modified gravity theory. This is in contrast with the self-accelerating branch of the DGP model (hereafter sDGP) where there exists a ghost at the linearised level (for a review see [10]). Another advantage of the model is that there is a mechanism to recover general relativity on small scales. Thus with this model we can modify gravity on large scales significantly without spoiling the success of general relativity on the solar system scales, providing the basis for the test of the large distance modification of general relativity.

In this paper, we study the phenomenological consequences of the normal branch DGP model (hereafter nDGP). We first present in Section II the geometrical tests on nDGP, looking for a parameter space which can be tested from structure formation, which is summarised in Section III. Then we present the ISW-galaxy correlations as a powerful tool to distinguish between LCDM and nDGP models in Section IV. Section V is devoted to the conclusion.

## II. GEOMETRICAL TESTS

The cosmic expansion of the nDGP model depends on the usual 4D FRW metric plus the gravitational effect of the 5D bulk on the brane. The cosmic acceleration is then introduced by the brane tension, which works as a cosmological constant on the brane. The gravity at large scales is modified by the 5D gravity effects on the brane, which are parameterised by a transition scale from 4D gravity to 5D gravity. The crossover distance  $r_c$  is defined as the ratio between 4D and 5D Planck mass scales

$$r_c = \frac{M_4^2}{2M_5^3}, \quad (1)$$

where  $M_4$  and  $M_5$  are the Planck scales in the 4D and 5D spacetime respectively. The late time expansion history is determined by two free parameters, the cosmological constant (or brane tension)  $\Lambda$  and the crossover distance  $r_c$ .

<sup>\*</sup>Tommaso.Giannantonio@port.ac.uk

<sup>†</sup>Yong-seon.Song@port.ac.uk

<sup>‡</sup>Kazuya.Koyama@port.ac.uk

The Friedmann equation for an nDGP model with curvature  $K = -\Omega_k H_0^2$  is given by

$$H^2 - \frac{\Omega_k H_0^2}{a^2} + \frac{1}{r_c} \sqrt{H^2 - \frac{\Omega_k H_0^2}{a^2}} = \frac{8\pi G}{3} \rho_m + \frac{\Lambda}{3}, \quad (2)$$

and the dimensionless expansion history  $E(a)$  is defined by

$$E^2(a) \equiv \frac{H^2(a)}{H_0^2} = \frac{\Omega_k}{a^2} + \left[ \sqrt{\frac{\Omega_m}{a^3} + \Omega_\Lambda + \Omega_{r_c}} - \sqrt{\Omega_{r_c}} \right]^2, \quad (3)$$

where  $\Omega_\Lambda = \Lambda/3H_0^2$  and  $\Omega_{r_c} = (4H_0^2 r_c^2)^{-1}$ , which satisfies

$$\sqrt{\Omega_{r_c}} = \frac{\Omega_m + \Omega_\Lambda + \Omega_k - 1}{2\sqrt{1 - \Omega_k}}. \quad (4)$$

The free parameter  $r_c$  can range in theory from 0 to the infinity; however, it has been shown that the deviations from general relativity on solar system scales are also controlled by  $r_c$ , and the current constraints require that  $r_c > H_0^{-1}$ . We can see that if  $r_c$  approaches the infinity, then Eq. (2) converges to GR, while if  $r_c$  approaches  $H_0^{-1}$ , then the 5D gravitational effect on the expansion history becomes maximal.

The modification of gravity at late time screens the cosmological constant and makes the effective equation of state less than  $-1$ . We define the effective energy density of dark energy  $\rho_{\text{eff}}$  as [11]

$$H^2 - \frac{\Omega_k H_0^2}{a^2} = \frac{8\pi G}{3} \rho_m + \frac{8\pi G}{3} \rho_{\text{eff}}$$

$$\rho_{\text{eff}} = \frac{1}{8\pi G} \left( \Lambda - \frac{3}{r_c} \sqrt{H^2 - \frac{\Omega_k H_0^2}{a^2}} \right). \quad (5)$$

It is clearly seen that the 5D effects make the effective dark energy density  $\rho_{\text{eff}}$  smaller. From the continuity equation of  $\rho_{\text{eff}}$

$$\dot{\rho}_{\text{eff}} + 3H(1 + w_{\text{eff}})\rho_{\text{eff}} = 0, \quad (6)$$

we can derive  $w_{\text{eff}}$  as

$$w_{\text{eff}} = -1 - \frac{\sqrt{\Omega_{r_c}} \Omega_m a^{-3}}{\Omega_\Lambda - 2\sqrt{\Omega_{r_c}}(E^2 - \Omega_k/a^2)^{1/2}}$$

$$\times \frac{1}{(E^2 - \Omega_k/a^2)^{1/2} + \sqrt{\Omega_{r_c}}}. \quad (7)$$

At the current time, the effective equation of state becomes

$$w_{\text{eff}}(a=1) = -1 - \frac{(\Omega_m + \Omega_\Lambda - 1)\Omega_m}{(1 - \Omega_m)(\Omega_m + \Omega_\Lambda + 1)}, \quad (8)$$

where we neglected the curvature for simplicity. Provided that  $\Omega_m < 1$ , we have the phantom behaviour  $w_{\text{eff}} < -1$ .

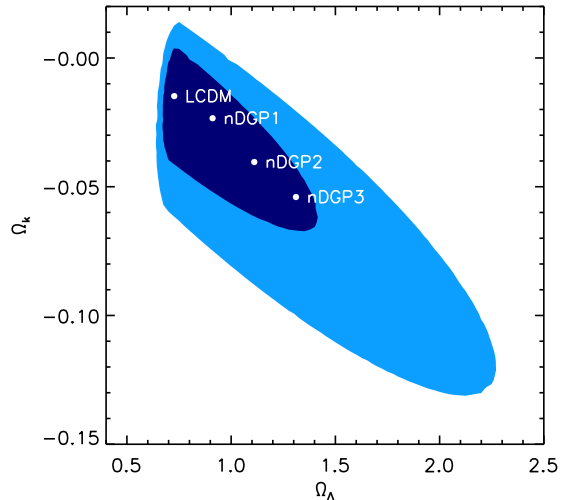


FIG. 1: Geometrical test on the nDGP by using SN+CMB+ $H_0$  observations. There is correlation observed in the projected  $\Omega_k$  and  $\Omega_\Lambda$  plane after marginalisation of all other cosmological parameters.

We revisit the geometrical test on the nDGP [11, 12]. The geometrical test on the nDGP with a flat curvature prior is not in favour of the cases for the significant screening effect, which rules out observable modified gravity effects in the nDGP. However we find that measurable screening effects are allowed with the inclusion of curvature. We exploit the leverage arm in the geometrical tests at both ends of low and high redshifts. At low redshifts, we use the Gold SN data set [13]. At high redshifts, we fix the distance to the last scattering surface at  $z_{\text{lss}} = 1088_{-2}^{+1}$  by fitting the harmonic space scale of the acoustic peak  $l^A = 302_{-1.4}^{+0.9}$  and matter density  $\Omega_m h^2 = 0.1268_{-0.0095}^{+0.0072}$  [14]. In addition to that, we constrain the expansion constant  $H_0$  with the Hubble constant measurement,  $H_0 = 72_{-8}^{+8}$  [15].

With a fixed CMB prior of  $\Omega_m h^2$ , best fit values for  $w$  and  $H_0$  are correlated with each other. The theoretical models predicting  $w < -1$  have a smaller best fit value for  $H_0$  compared with LCDM ( $w = -1$ ). Since the measured comoving distance to  $z_{\text{lss}}$  is consistent with a best fit value for  $H_0$  in flat LCDM, the comoving distance to  $z_{\text{lss}}$  in phantom-like braneworld models becomes longer than the measured distance. This worse fit for the large distance measured by CMB in the models with  $w < -1$  can be cured by introducing a positive curvature which makes the distance shorter without significantly affecting the fit for the shorter distance measured by SNe. Consequently, a larger  $\Omega_\Lambda$ , which realises larger screening effects and  $w < -1$ , is allowed with a positive curvature ( $\Omega_k < 0$ ) as is shown in Fig. 1. Hence if the curvature is added, there appears a degeneracy in the geometrical tests and the models with large modified gravity effects

are allowed. This degeneracy can be broken by the structure formation test.

### III. STRUCTURE FORMATION TESTS

There are three regimes of gravity in the nDGP model on different scales. On super-horizon scales, gravity is significantly influenced by 5D effects. In this regime, we cannot ignore the time evolution of metric perturbations and the dynamical solutions should be obtained by solving the 5D equations of motion. The dynamical solutions have been obtained in the following two methods in the literature: a first derivation is obtained by the scaling ansatz in the sDGP [16] and in the nDGP [17], and the other is found from the full 5D numerical simulations [18]. It has been shown that both approaches give identical results, and the solutions for the perturbations are shown to be insensitive to the initial conditions for the 5D metric perturbations.

On sub-horizon scales, we can ignore the time dependence of the metric perturbations and the quasi-static approximations can be used [19, 20]. Even on scales smaller than  $r_c$ , gravity is not described by general relativity due to an extra scalar degree of freedom introduced by the modification of gravity. In this regime, gravity can be described by a Brans-Dicke theory and the growth of structure becomes scale independent.

We use the Newtonian gauge

$$ds^2 = -(1 + 2\Psi) dt^2 + a(t)^2(1 + 2\Phi) \delta_{ij} dx^i dx^j, \quad (9)$$

to describe the metric perturbations. Fig. 2 shows the behaviour of metric perturbations  $\Phi_- \equiv (\Phi - \Psi)/2$  which determines the integrated Sachs-Wolfe (ISW) effect both for the dynamical solutions and scaling solutions, for the models of Table I. In the literature, the spatial curvature was not introduced in the calculations, and thus we derive the quasi-static solutions with curvature in Appendix A.

	LCDM	nDGP 1	nDGP 2	nDGP 3
$\Omega_m$	0.30	0.32	0.34	0.37
$\Omega_b$	0.052	0.056	0.060	0.064
$\Omega_k$	-0.014	-0.027	-0.040	-0.053
$\Omega_\Lambda$	0.72	0.90	1.1	1.3
$H_0$	66	63	61	59

TABLE I: Details of the cosmological models used. The other parameters are for all models: scalar spectral index  $n_s = 0.95$ , optical depth  $\tau = 0.10$ , and amplitude of the primordial scalar perturbations  $A = 2.04 \cdot 10^{-9}$  at a pivot scale  $k = 0.05 \text{ Mpc}^{-1}$ .

Finally, once the non-linearity of density perturbations becomes important, the theory approaches general relativity [19, 21]. This transition to general relativity is crucial to satisfy the tight constraints from the solar system experiments [22, 23], and will play a crucial role for weak lensing measures. On the other hand, for the ISW effect, we can safely ignore the non-linear physics.

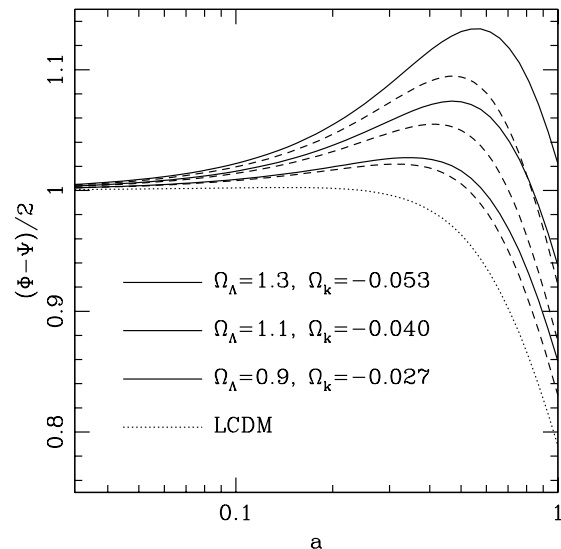


FIG. 2: We plot the solutions of structure formation of three nDGP models in the  $1 - \sigma$  contour of Fig. 1, compared with the LCDM (dotted line). Solid curves represent the quasi-static solutions of nDGP models with different  $\Omega_\Lambda$ , and the dashed curve attached to each solid curve represents the dynamic solution of each nDGP model at  $k = 10^{-3} \text{ Mpc}^{-1}$ .

The dynamical solutions are relevant to the scales of the large scales CMB anisotropies. We have checked that the difference in the large scales CMB anisotropies from LCDM are small given the constraints from the geometrical tests because, due to the large cosmic variance, we do not expect that the CMB anisotropies on these scales can give strong constraints on the models. The quasi-static solutions are relevant to the scales of ISW-galaxy cross-correlations. In the next section, we will study how they can be used to break the degeneracy that arises from the geometrical tests.

### IV. ISW-GALAXY CORRELATIONS

The gravitational potential well  $\Phi_-$  is shallower in the nDGP model than in the LCDM model due to the modification of gravity. This is the opposite from what happens in the self-accelerating models [24] where the gravitational potential well is deeper than in LCDM. The nDGP model predicts an earlier variation of the gravitational potential than the LCDM model. By cross-correlating galaxies at different redshifts with the CMB, one can in principle trace the redshift history of the decay of the potential. Furthermore, the cross-correlation arises from the well understood quasi-static (QS) regime of nDGP (solid curves in Fig. 2).

The cross-power spectrum of the CMB and a set of

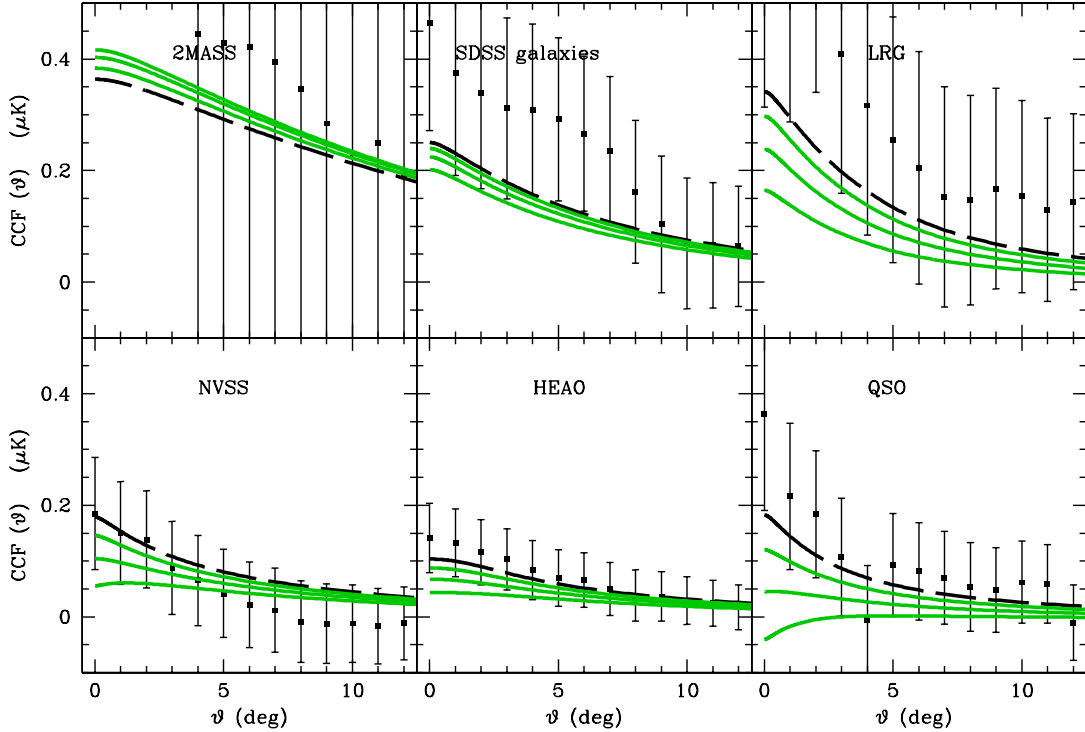


FIG. 3: Measurement of the cross-correlation functions between six different galaxy data sets and the CMB, reproduced from [2]. The curves show the theoretical predictions for the ISW-galaxy correlations at each redshift for the LCDM model (black, dashed) and the three nDGP models of Fig. 2 (green, solid), which describe the  $1 - \sigma$  region of the geometry test from Fig. 1.

galaxies  $g_i$  is given by [25, 26]

$$C_l^{I g_i} = 4\pi \int \frac{dk}{k} I_l^I(k) I_l^{g_i}(k) \frac{k^3 P_{\Phi_- \Phi_-}(k, 0)}{2\pi^2}, \quad (10)$$

where  $P_{\Phi_- \Phi_-}(k, 0)$  is the power spectrum of  $\Phi_-$  at the present time and the kernel  $I_l^I$  is

$$I_l^I(k) = \int dz W^I(k, z) j_l(kD) \left( \frac{dD}{dr} \right)^{1/2}. \quad (11)$$

The window function is given by

$$W^I(k, z) = -\frac{2}{1+z} \frac{\partial}{\partial \ln a} \left[ \frac{\Phi_-(k, z)}{\Phi_-(k, 0)} \right], \quad (12)$$

where the galaxy kernel  $I_l^{g_i}$  is

$$I_l^{g_i}(k) = \int dz W^{g_i}(k, z) j_l(kD) \left( \frac{dD}{dr} \right)^{1/2}. \quad (13)$$

Under the QS approximation, the window function becomes

$$W^{g_i}(k, z) = \frac{2}{3\Omega_m H_0^2} \frac{n_i(z) b_i(z)}{1+z} \frac{\Phi_-(k, z)}{\Phi_-(k, 0)}, \quad (14)$$

where  $n_i(z)$  is the redshift distribution of the galaxies normalised to  $\int dz n_i = 1$  and  $b_i(z)$  is the galaxy bias.

First, we investigate the current status of the observations using the data set obtained in [2], which consists in the measurement of the ISW effect via the real space cross-correlation functions (CCF) between six different galaxy catalogues and the CMB. The redshift distributions of the different catalogues are partly overlapping, but each data set  $i$  is characterised by a median redshift  $0.1 \leq \bar{z}_i \leq 1.5$  around which each particular measured CCF is getting the biggest contribution. Thus, this analysis represents a first step towards an exploration of the redshift evolution of the potentials and, ultimately, of gravity itself as described by [27].

We reproduce in Fig. 3 the measured CCF for the six galaxy catalogues from [2], in order of increasing redshift: 2MASS (excluding the small scale contaminated data), the main galaxy sample from the SDSS, the SDSS Luminous Red Galaxies, NVSS, HEAO and the SDSS quasars, with the relative error bars which should be remembered are highly correlated. Looking at the theoretical curves in Fig. 3, we can see that the nDGP models have a very different prediction from the LCDM for the CCF at high redshift. This is in agreement with their peculiar potential evolution: the rise in the potential  $\Phi_-$  at high

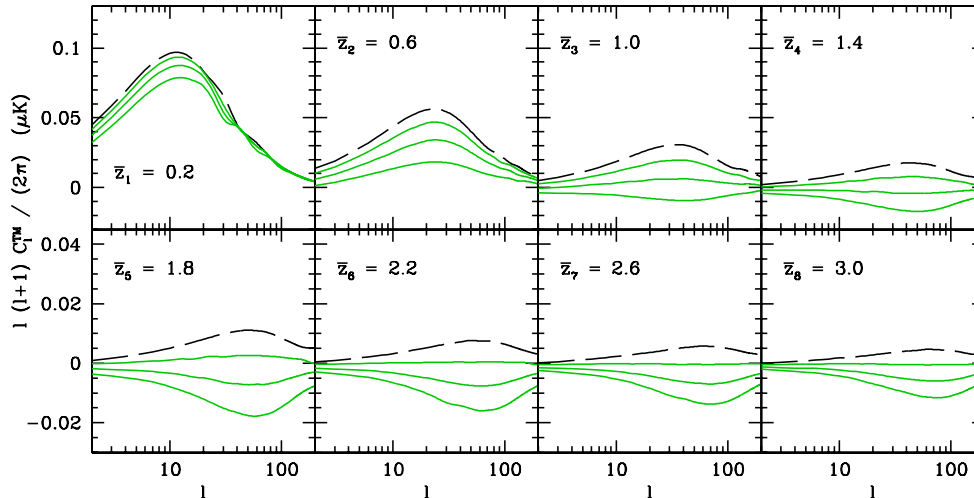


FIG. 4: The theoretical predictions for the ISW-galaxy cross power spectra at each redshift for the LCDM model (black, dashed) and the three nDGP models of Fig. 2 (green, solid), which describe the  $1 - \sigma$  region of the geometry test from Fig. 1.

redshift produces an expected negative CCF, while the following steeper decay leads to a positive CCF which becomes eventually higher than the LCDM one.

However, it is clear that these predictions represent a poor fit to the high redshift data. Remembering that all three nDGP models in Fig. 3 are inside the  $1\sigma$  region from the geometry test of Section II, we can qualitatively see that the ISW test will produce stricter constraints by noticing e.g. that the quasar CCF alone has a significance level of  $2\sigma$ , which means that at least two of the nDGP models will be excluded at above this level.

Then, we study the best possible constraints which can be obtained by this technique with future surveys. For definiteness, we assume that the galaxy sets come from a net galaxy distributions of

$$n_g(z) \propto z^2 e^{-(z/1.5)^2}, \quad (15)$$

where the normalisation is given by the LSST expectation of 35 galaxies per arcmin<sup>2</sup>. For the subsets of galaxies, we assume that this total distribution is separated by photometric redshifts which have a Gaussian error distribution with rms  $\sigma(z) = 0.03(1+z)$ . The redshift distributions are then given by [27]

$$n_i(z) = \frac{A_i}{2} n_g(z) \left[ \operatorname{erfc} \left( \frac{z_{i-1} - z}{\sqrt{2}\sigma(z)} \right) - \operatorname{erfc} \left( \frac{z_i - z}{\sqrt{2}\sigma(z)} \right) \right],$$

where  $\operatorname{erfc}$  is the complementary error function and  $A_i$  is determined by the normalisation constraint.

We show in Fig. 4 the predicted cross power spectra obtained using this redshift tomography for the models of Table I. The theoretical possibility to distinguish be-

tween them is given by the signal to noise ratio

$$\left( \frac{S}{N} \right)^2 = \sum_l f_{\text{sky}} (2l+1) \frac{[C_l^{Ig}]^2}{C_l^{gg} C_l^{TT} + [C_l^{Ig}]^2}, \quad (16)$$

where  $C_l^{TT}$  is the temperature power spectrum. This is summarised in Table II.

$\bar{z}$	LCDM	nDGP 1	nDGP 2	nDGP 3
0.2	2.8	2.9	2.6	2.2
0.6	4.0	3.5	2.5	1.3
1.0	3.4	2.2	0.68	1.1
1.4	2.5	1.2	0.69	2.6
1.8	1.9	0.52	1.3	3.2
2.2	1.5	0.16	1.6	3.3
2.6	2.4	0.18	1.6	3.1
3.0	0.96	0.22	1.5	2.9

TABLE II: Theoretical signal to noise ratio for the models of Table I with  $f_{\text{sky}} = 1$ .

Although the geometrical test is not able to easily break the degeneracy between curvature and the screening effect, the alternative consequence for the structure formation by the screening effect is measurable from the ISW-galaxy cross-correlations. The screening of the cosmological constant in nDGP2 and nDGP3 becomes effective before the decay of the growth factor which occurs when the matter component becomes subdominant. This early screening enhances the growth factor which makes the potential  $\Phi_-$  grow. This generates anti-correlations in the ISW-galaxy cross-correlations at high redshifts, which leaves observable signatures as is shown in Fig. 4.

From Table II, it is expected that this effect on the structure formation can be observed at around 50% noise level for nDGP2 and 25% noise level for nDGP3. This is an illustration how we can break the degeneracy between curvature and the screening effect in the geometrical tests by using the structure formation tests.

## V. CONCLUSION

In this paper, we studied the observational constraints on the normal branch DGP model in which a phantom-like behaviour occurs only with cold dark matter and a cosmological constant. The geometrical tests using the gold SN data set, CMB and the HST key project are not enough to rule out models in which gravity is significantly modified on cosmological scales. We then showed that the structure formation tests performed using the integrated Sachs-Wolfe (ISW) effect can break the degeneracy in the parameter space.

The current measurements of the ISW effect obtained in [2] are indeed as competitive as the geometrical tests. This is due to the fact that, in the nDGP model, the cross-correlation with galaxies becomes negative at high redshift due to the peculiar behaviour of the metric perturbations caused by the modification of gravity. This demonstrates that the structure formation tests are very promising tools to distinguish between general relativity and modified gravity models. We also showed that it is possible to track the evolution of the potentials by cross-correlating the ISW with galaxies at each redshift in future observations. It is very likely that in the future the ISW effect will provide one of the strongest constraints on the model. We will present the full likelihood analysis using the latest data sets in a forthcoming paper.

### Acknowledgements

We would like to thank Robert Crittenden, Roy Maartens and Elisabetta Majerotto for useful discussion. YS and KK are supported by STFC.

## APPENDIX A: QUASI-STATIC SOLUTIONS WITH CURVATURE

In the Gaussian normal coordinates, the 5D metric is given by [22]

$$ds^2 = dy^2 - n(y, t)^2 dt^2 + a(y, t)^2 \delta_{ij} dx^i dx^j, \quad (\text{A1})$$

where

$$a(y, t) = a(t) \left[ 1 - \left( H^2 - \frac{\Omega_k}{a_0^2} \right)^{\frac{1}{2}} y \right], \quad (\text{A2})$$

$$n(y, t) = 1 - (\dot{H} + H^2) \left( H^2 - \frac{\Omega_k}{a_0^2} \right)^{-\frac{1}{2}} y. \quad (\text{A3})$$

The extrinsic curvature of the brane is determined by the first derivative of the metric with respect to  $y$  at the brane ( $y = 0$ ):

$$\frac{a'}{a} = - \left( H^2 - \frac{\Omega_k}{a^2} \right)^{\frac{1}{2}}, \quad (\text{A4})$$

$$\frac{n'}{n} = - \left( \dot{H} + H^2 \right) \left( H^2 - \frac{\Omega_k}{a^2} \right)^{-\frac{1}{2}}. \quad (\text{A5})$$

Defining the comoving density perturbations

$$\rho \Delta = \delta \rho - 3H a \delta q, \quad (\text{A6})$$

the Poisson equation is obtained as

$$\frac{k^2}{a^2} \Phi = \frac{\kappa_4^2}{2} \left[ \frac{2(a'/a)r_c}{2(a'/a)r_c - 1} \right] \left[ \rho \Delta - \frac{\delta \rho_E - 3H a \delta q_E}{2(a'/a)r_c} \right]. \quad (\text{A7})$$

The traceless part of the space-space component of the effective Einstein equations gives

$$\begin{aligned} & -\frac{1}{a^2} \left\{ 1 - \frac{1}{r_c [(a'/a) + (n'/n)]} \right\} (\Phi + \Psi) \\ & = -\frac{\kappa_4^2 \delta \pi_E}{r_c [(a'/a) + (n'/n)]}. \end{aligned} \quad (\text{A8})$$

The Weyl density perturbations  $\delta \rho_E$ ,  $\delta q_E$  and  $\delta \pi_E$  should be determined by the constraint equations

$$\dot{\delta \rho}_E + 4H \delta \rho_E - a^{-1} k^2 \delta q_E = 0, \quad (\text{A9})$$

$$\begin{aligned} \dot{\delta q}_E + 4H \delta q_E + a^{-1} \left( \frac{1}{3} \delta \rho_E - \frac{2}{3} k^2 \delta \pi_E \right) \\ = -a^{-1} \frac{2}{3} r_c \left( \frac{n'}{n} - \frac{a'}{a} \right) \left\{ -\frac{\rho \Delta}{2(a'/a)r_c - 1} \right. \\ + \frac{\delta \rho_E - 3H a \delta q_E}{2(a'/a)r_c - 1} \\ \left. + \frac{1}{r_c [(a'/a) + (n'/n)] - 1} k^2 \delta \pi_E \right\}. \end{aligned} \quad (\text{A10})$$

The constraint equations are not closed and we need additional information by solving the 5D equation of motion. In the quasi-static limit, we can impose the condition on  $\delta \rho_E$  and  $\delta \pi_E$  from the bulk equation as [20]

$$\delta \rho_E = 2k^2 \delta \pi_E. \quad (\text{A11})$$

Then the constraint equations give

$$\delta \rho_E = 2 \left[ \frac{-1 + (a'/a)r_c + (n'/n)r_c}{-3 + 4(a'/a)r_c + 2(n'/n)r_c} \right] \rho \Delta, \quad (\text{A12})$$

and  $\delta q_E = 0$ . The Poisson equation and the traceless part of Einstein equations give

$$\frac{k^2}{a^2} \Phi = \frac{\kappa_4^2}{2} \left[ 1 - \frac{1}{3\beta(t)} \right] \rho \Delta, \quad (\text{A13})$$

$$\frac{k^2}{a^2} \Psi = -\frac{\kappa_4^2}{2} \left[ 1 + \frac{1}{3\beta(t)} \right] \rho \Delta, \quad (\text{A14})$$

where

$$\beta(t) = 1 - \frac{2}{3} \left[ 2 \left( \frac{a'}{a} \right) + \left( \frac{n'}{n} \right) \right] r_c, \quad (\text{A15})$$

which can be written as

$$\beta(t) = 1 + 2H^2 r_c \left( H^2 - \frac{\Omega_k}{a^2} \right)^{-1/2} \left[ 1 + \frac{\dot{H}}{3H^2} - \frac{2}{3} \frac{\Omega_k}{a^2 H^2} \right]. \quad (\text{A16})$$

- 
- [1] W. J. Percival et al., *Mon. Not. Roy. Astron. Soc.* **381**, 1053 (2007), arXiv:0705.3323 [astro-ph].
- [2] T. Giannantonio et al. (2008), arXiv:0801.4380 [astro-ph].
- [3] R. R. Caldwell, *Phys. Lett.* **B545**, 23 (2002), astro-ph/9908168.
- [4] C. Csaki, N. Kaloper, and J. Terning, *JCAP* **0606**, 022 (2006), astro-ph/0507148.
- [5] M. Libanov, V. Rubakov, E. Papantonopoulos, M. Sami, and S. Tsujikawa, *JCAP* **0708**, 010 (2007), arXiv:0704.1848 [hep-th].
- [6] V. Sahni and Y. Shtanov, *JCAP* **0311**, 014 (2003), astro-ph/0202346.
- [7] A. Lue and G. D. Starkman, *Phys. Rev.* **D70**, 101501 (2004), astro-ph/0408246.
- [8] G. R. Dvali, G. Gabadadze, and M. Porrati, *Phys. Lett.* **B485**, 208 (2000), hep-th/0005016.
- [9] C. Deffayet, *Phys. Lett.* **B502**, 199 (2001), hep-th/0010186.
- [10] K. Koyama (2007), arXiv:0709.2399 [hep-th].
- [11] R. Lazkoz, R. Maartens, and E. Majerotto, *Phys. Rev.* **D74**, 083510 (2006), astro-ph/0605701.
- [12] R. Lazkoz and E. Majerotto, *JCAP* **0707**, 015 (2007), arXiv:0704.2606 [astro-ph].
- [13] A. G. Riess et al. (Supernova Search Team), *Astrophys. J.* **607**, 665 (2004), astro-ph/0402512.
- [14] D. N. Spergel et al. (WMAP), *Astrophys. J. Suppl.* **148**, 175 (2003), astro-ph/0302209.
- [15] W. L. Freedman et al. (HST), *Astrophys. J.* **553**, 47 (2001), astro-ph/0012376.
- [16] I. Sawicki, Y.-S. Song, and W. Hu, *Phys. Rev.* **D75**, 064002 (2007), astro-ph/0606285.
- [17] Y.-S. Song (2007), arXiv:0711.2513 [astro-ph].
- [18] A. Cardoso, K. Koyama, S. S. Seahra, and F. P. Silva (2007), arXiv:0711.2563 [astro-ph].
- [19] A. Lue and G. Starkman, *Phys. Rev.* **D67**, 064002 (2003), astro-ph/0212083.
- [20] K. Koyama and R. Maartens, *JCAP* **0601**, 016 (2006), astro-ph/0511634.
- [21] K. Koyama and F. P. Silva, *Phys. Rev.* **D75**, 084040 (2007), hep-th/0702169.
- [22] C. Deffayet, G. R. Dvali, G. Gabadadze, and A. I. Vainshtein, *Phys. Rev.* **D65**, 044026 (2002), hep-th/0106001.
- [23] G. Dvali, A. Gruzinov, and M. Zaldarriaga, *Phys. Rev.* **D68**, 024012 (2003), hep-ph/0212069.
- [24] Y.-S. Song, I. Sawicki, and W. Hu, *Phys. Rev.* **D75**, 064003 (2007), astro-ph/0606286.
- [25] L. Pogosian, *JCAP* **0504**, 015 (2005), astro-ph/0409059.
- [26] P.-S. Corasaniti, T. Giannantonio, and A. Melchiorri, *Phys. Rev.* **D71**, 123521 (2005), astro-ph/0504115.
- [27] W. Hu and R. Scranton, *Phys. Rev.* **D70**, 123002 (2004), astro-ph/0408456.